## *Headline Articles*

# Cause for Unusually Large Thermal Hysteresis of Spin Crossover in $[Fe(2\text{-pic})_3]Cl_2 \cdot H_2O$#

**Tadahiro Nakamoto, Ashis Bhattacharjee,† and Michio Sorai***

Research Center for Molecular Thermodynamics, Graduate School of Science, Osaka University, Toyonaka, Osaka 560-0043

Received September 16, 2003; E-mail: sorai@chem.sci.osaka-u.ac.jp

Thermodynamic properties of an iron(II) spin crossover complex $[Fe(2\text{-pic})_3]Cl_2 \cdot H_2O$ (2-pic: 2-picolylamine or 2-aminomethylpyridine), for which an unusually large thermal hysteresis with a width of $[T_c(\uparrow) - T_c(\downarrow) = 91$ K] in its spin-state transition has been observed by $^{57}$Fe Mössbauer spectroscopy, were investigated by adiabatic heat capacity calorimetry. Contrary to the previous observation, the preliminary DTA result showed much smaller thermal hysteresis around 200 K, with a width of $[T_c(\uparrow) - T_c(\downarrow) = 12$ K]. The present heat capacity measurement by adiabatic calorimetry revealed that there exists a metastable low-spin low-temperature phase, besides the stable low-spin low-temperature phase and that this complex undergoes stabilization from the metastable low-spin phase to the stable low-spin phase accompanied by a large heat evolution when the sample is annealed around 200 K. The stable low-spin phase exhibited a phase transition to the high-spin high-temperature phase around 280 K upon heating. The high-spin state was found to be always undercooled down to ~200 K. The large thermal hysteresis earlier reported for the title complex turns out to be apparent and is caused by the existence of the metastable low-spin phase. Moreover, another intermediate metastable (low-spin?) phase was found when the sample in the metastable low-spin phase was heated from 150 K at a heating rate of ~5 K h$^{-1}$. This metastable phase exhibited a phase transition to the undercooled high-spin phase at ~265 K.

Temperature-induced spin crossover phenomena, in which the spin-state conversion between a low spin (LS) and a high spin (HS) state takes place during temperature change, have been widely investigated.[2–4] In the cases of octahedral iron(II) complexes for which the spin crossover phenomena have been extensively investigated, the iron ion undergoes the spin transition between low spin ($^1A_{1g}$, $S = 0$) at low temperatures and high spin ($^5T_{2g}$, $S = 2$) at high temperatures, where $S$ stands for the spin quantum number. The mechanism of this phenomenon at the molecular level can be understood in terms of an equilibrium fashion between the two electronic states, i.e., Le Chatelier–Brown's law. In the solid state, however, the situation is more complicated because the intermolecular interactions cannot be ignored. Furthermore, some characteristics of condensed matters such as mixing effect and lattice phase transition should also be taken into consideration.

In order to discuss the stability of a given phase, one should examine the Gibbs energy consisting of both the entropy $S$ and the enthalpy $H$ terms:

$$G = H - TS. \quad (1)$$

It has widely been accepted that the entropy change mainly consists of the electronic and the vibrational contributions and that the latter is much larger than the former.[5]

The temperature-induced spin crossover phenomena are usually classified into two types based on the temperature dependence of the high-spin fraction: One is the so-called "*discontinuous type*", in which the spin state conversion between the LS and the HS states takes place accompanied by a thermal hysteresis, and the other is the so-called "*continuous type*", in which the spin state conversion takes place without hysteresis. Normally, the continuous type of spin crossover phenomenon is accompanied by no change in the macroscopic symmetry of the crystal, while the discontinuous type is accompanied by a crystallographic change. This is strongly suggestive of the relationship between the discontinuity in spin crossover phenomenon and the structural phase transition, although a few exceptions are known. There is also another classification based on the wideness of temperature range of the spin transition, i.e., one is the "*abrupt type*" in which the spin state conversion between the LS and the HS states takes place within a narrow temperature range (< ~10 K) and often accompanied by a hysteresis and the other is the "*gradual type*" in which the spin state conversion takes place over a wider temperature range than ~100 K, although it is not easy to draw a strict demarcation between them. Although the two classifications often become phenom-

† Present address: Department of Physics, St. Joseph's College (University Section), North Point, Darjeeling, West Bengal 734101, India

Published on the web May 6, 2004; DOI 10.1246/bcsj.77.921

enologically synonymous with each other, i.e., discontinuous type = abrupt type and continuous type = gradual type, some exceptions are known.

In 1984 Gütlich and his collaborators[6] discovered the LIESST (Light Induced Excited Spin State Trapping) phenomenon, occurring at lower temperatures than the material's thermal spin transition temperature. The transition from a LS state to a HS state is induced by light irradiation, so the excited metastable HS state can be trapped for a long time even after the light irradiation is stopped. After this discovery, the spin crossover system has been highlighted as a possible candidate of molecular switching devices. On the other hand, a spin crossover system which exhibits a large thermal hysteresis is also sought. Since such a system may show a marked bistability against temperature fluctuations, this phenomenon can be used as a memory device. If room temperature falls in the range of the hysteresis loop, such a system will provide a practical use at ambient temperature. A system $[Fe(Htrz)_{2.85}(4\text{-}NH_2trz)_{0.15}](ClO_4)_2 \cdot nH_2O$, where Htrz is 4*H*-1,2,4-triazole and 4-$NH_2$trz is 4-amino-1,2,4-triazole,[7] was found to exhibit a spin transition with a hysteresis loop [$T_c(\uparrow) = 304$ K and $T_c(\downarrow) = 288$ K] in which room temperature is involved, although the width of the thermal hysteresis is not so large: $T_c(\uparrow) - T_c(\downarrow) = 16$ K.

The thermal hysteresis is characteristic of a first-order phase transition and the type of transition is usually abrupt and discontinuous. The width of the hysteresis seen in the spin crossover phase transition has been usually ~40 K at most.[8] However, an iron(II) spin crossover complex $[Fe(2\text{-pic})_3]Cl_2 \cdot H_2O$ (2-pic: 2-picolylamine or 2-aminomethylpyridine) is known to give rise to a spin crossover phase transition with an unusually large thermal hysteresis.[9] The temperature dependence of the high-spin area fraction ($f_{HS}$) of the $^{57}$Fe Mössbauer spectra of this complex is reproduced in Fig. 1. The transition temperature defined as $f_{HS} = 0.5$ is $T_c(\uparrow) = 290$ K and $T_c(\downarrow) = 199$ K. Such a large thermal hysteresis with $T_c(\uparrow) - T_c(\downarrow) = 91$ K for the spin state transition has never been known in any other systems. It should be emphasized here that this large thermal hysteresis is not caused by dehydration from the monohydrate owing to the phase transition occurring at some higher temperature.

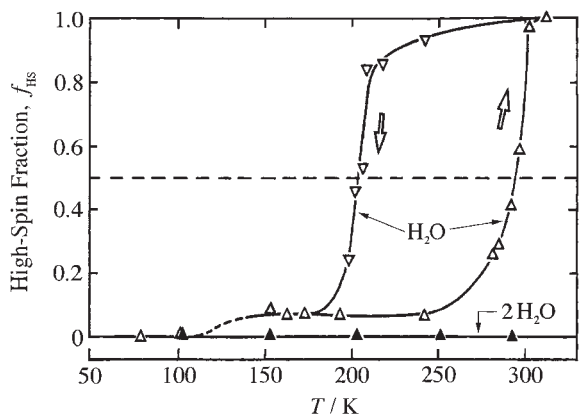


Fig. 1. Temperature dependence of the high spin area fraction $f_{HS}$ of the $^{57}$Fe Mössbauer spectra of $[Fe(2\text{-pic})_3]Cl_2 \cdot H_2O$ and the low spin dihydrate $[Fe(2\text{-pic})_3]Cl_2 \cdot 2H_2O$.[9]

The purpose of the present study is to measure the heat capacity by adiabatic calorimetry and to elucidate the cause for the unusually large thermal hysteresis of the spin crossover phenomenon.

## Experimental

**Compound Preparation.** The sample was prepared by the method previously reported with slight modifications.[10,11]

**$[Fe(2\text{-pic})_3]Cl_2 \cdot 2H_2O$.** To a concentrated iron(III)-free aqueous solution of $FeCl_2 \cdot 4H_2O$, 3 equivalents of 2-aminomethylpyridine (2-picolylamine) was added. The dark red crystals, that were formed after slow evaporation under nitrogen stream, were filtered off, washed with 2-butoxyethanol and acetone, and then dried under a nitrogen stream. Anal. Found: C, 44.47; H, 5.81; N, 17.45%. Calcd for $C_{18}H_{28}N_6O_2FeCl_2$: C, 44.37; H, 5.79; N, 17.24%.

**$[Fe(2\text{-pic})_3]Cl_2 \cdot H_2O$.** The monohydrate was prepared by partial dehydration of the dihydrate under helium stream at ca. 80 °C on a water bath until dark red crystals completely turned into yellow powder. This compound easily absorbs moisture to become the dihydrate when it is exposed to air, as evidenced by the immediate color change to red. Anal. Found: C, 46.22; H, 5.60; N, 17.95%. Calcd for $C_{18}H_{26}N_6OFeCl_2$: C, 46.07; H, 5.58; N, 17.91%.

**Preliminary Thermal Analysis (DTA).** Preliminary observation of the thermal properties was made with a home-built DTA apparatus.

**Heat Capacity Measurements.** Heat capacity measurements between 12 and 350 K were made with a home-built adiabatic calorimeter.[12] Because of the unexpectedly complicated thermal behavior of this complex described below, two specimens (named A and B) from different batches were needed. The specimen A was used for usual heat capacity measurements, while the specimen B was mainly used for the sake of determination of the enthalpy relation between the stable and the metastable phases. The mass of specimen A was 4.05746 g (8.64780 mmol) and that of specimen B was 4.35083 g (9.27286 mmol). A small amount of helium gas (59 kPa at room temperature) was sealed in the calorimeter cell to aid the heat transfer. The thermometer mounted on the calorimeter vessel was a platinum resistance thermometer (Minco Product, S1055), of which the temperature scale is based upon the IPTS-68. Although there exists a difference between the ITS-90 and IPTS-68 at low temperatures, the difference is small and is smooth above room temperature till about 600 K.[13] The heat capacities determined here have not been adjusted by correcting the IPTS-68 value to the ITS-90 value.

## Results

**Preliminary DTA Measurements for Specimen A.** The preliminary DTA thermograms for $[Fe(2\text{-pic})_3]Cl_2 \cdot H_2O$ are shown in Fig. 2. Upon cooling, the DTA thermogram exhibited an exothermic thermal anomaly at $T_c(\downarrow) = 199$ K, which is in good agreement with the transition temperature determined by $^{57}$Fe Mössbauer spectroscopy[9] (Fig. 1). On the other hand, the DTA thermogram upon heating showed an endothermic thermal anomaly at $T_c(\uparrow) = 211$ K, which is much lower than that determined by the $^{57}$Fe Mössbauer spectroscopy $T_c(\uparrow) = 295$ K. The width of the thermal hysteresis determined by DTA measurement was only a usual value, $T_c(\uparrow) - T_c(\downarrow) = 12$ K. DTA measurements done for three specimens from different batches also gave rise to a similar width of the hysteresis. Although the reason for this discrepancy between the former Mössbauer result and the present DTA result was not clear at

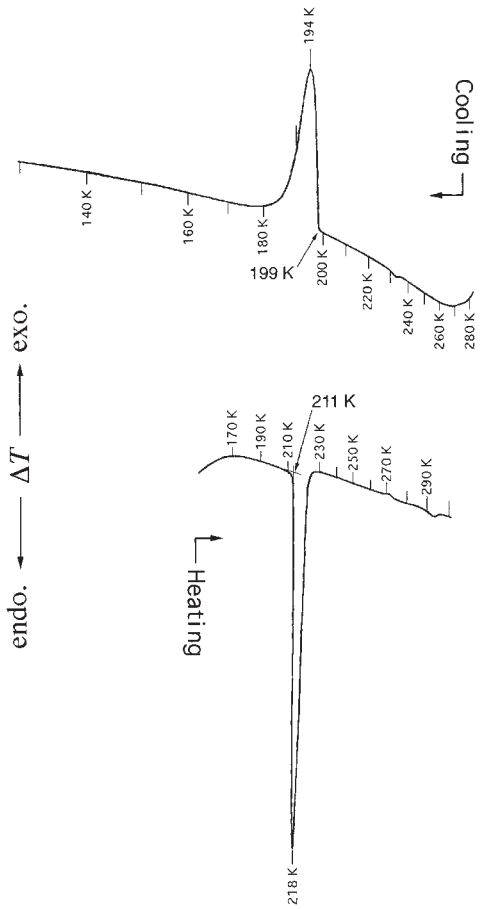


Fig. 2. DTA thermograms of $[Fe(2\text{-pic})_3]Cl_2 \cdot H_2O$ (specimen A). The cooling and heating rates are ca. 5 K min$^{-1}$ and ca. 7 K min$^{-1}$, respectively.

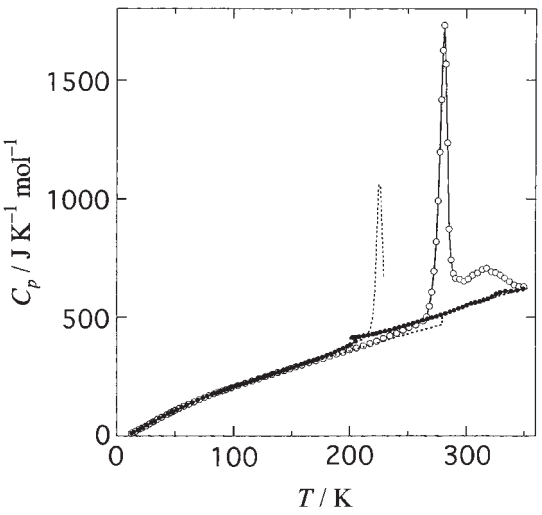


Fig. 3. Plot of molar heat capacity of $[Fe(2\text{-pic})_3]Cl_2 \cdot H_2O$ (specimen A) vs temperature. Open circles are the $C_p$ data for the stable LS and HS phases. Solid circles above and below 205 K indicate the $C_p$ values for the undercooled HS phase and the metastable LS phase (1), respectively. The dotted line indicates the $C_p$ values measured by the continuous heating method. The broken curve shows the estimated normal heat capacity $C_{lat}$ for the stable LS phase (see text).

this stage, we decided to measure the heat capacity of the specimen A, because the chemical purity did not seem to present any problem.

**Heat Capacity Measurement for Specimen A.** The molar heat capacities under constant pressure, $C_p$, of the monohydrate (specimen A) at temperatures between 12 K and 350 K are plotted in Fig. 3 and listed in Tables 1 and 2. The sample was slowly cooled from room temperature down to below $T_c(\downarrow)$. During the cooling process, it was checked by monitoring the temperature of the calorimeter vessel as a function of time that the phase transition occurred at ~200 K. Then the sample was heated up to ~200 K and the temperature was held at ~200 K in order to anneal the specimen in the LS phase for more than 2 weeks until the small heat evolution calmed down. This small heat evolution originated from the stabilization within the identical LS phase. The heat capacity of the specimen thus treated was successfully measured from 12 K to ~200 K for the LS state, as plotted in Fig. 3 by solid circles. The $C_p$ data obviously curve to an upper value at ~200 K, implying a symptom of a phase transition from the LS phase to the HS phase. However, when the temperature reached to ~205 K, a vigorous heat evolution occurred while waiting for the thermal equilibration after a Joule-energy input to the calorimeter vessel and the sample temperature eventually rose more than 10 K. As described below, this unexpected spontaneous heat evolution turned out to arise from the stabilization from the LS phase to a more stable LS phase. Unfortunately, the precise temperature change of the sample could not be traced during this heat evolution under the adiabatic condition, so that the relation of the enthalpy between the metastable LS state and the stable LS state could not be determined for the specimen A.

After waiting for the termination of the vigorous heat evolution, we checked whether the phase transition at ~200 K still existed and confirmed the absence of a phase transition by temperature monitoring upon cooling. The $C_p$ measurement at temperatures around 200 K also indicated the absence of the phase transition and smaller $C_p$ values than those before stabilization. These facts imply that the sample changed into a more stable phase (obviously LS phase) from the previous LS phase owing to the stabilization. We then performed heat capacity measurement for the new phase, i.e., the stable LS phase, from the lowest temperature (~12 K). The data indicated by open circles in Fig. 3 are the heat capacities of the stable LS phase and the consequent HS phase. The $C_p$ values of the stable LS phase are almost the same as those of the metastable LS phase below ~150 K, but a discrepancy starts at ~150 K and becomes remarkable above ~200 K at which the phase transition of the metastable LS phase occurs. The heat capacity of the stable LS phase exhibited no anomalies at ~200 K, but exhibited a large phase transition at 280.79 K ($T_{trs1}$). This temperature is very close to the $T_c(\uparrow)$ determined by the $^{57}$Fe Mössbauer spectroscopy.[9] An additional heat capacity hump was observed above this phase transition, which seems to terminate at ~350 K.

As we know, on the basis of preliminary DTA and DSC measurements, that the HS phase is easily undercooled through the phase transition temperature 280.79 K, we tried to measure heat capacities of the undercooled HS phase. Since it is usually

Table 1. Molar Heat Capacities of the Stable LS and the HS Phases of the Spin Crossover Complex $[Fe(2\text{-pic})_3]Cl_2 \cdot H_2O$ (Specimen A, Relative Molar Mass 483.22)

| $T$ | $C_p$ | $T$ | $C_p$ | $T$ | $C_p$ | $T$ | $C_p$ | $T$ | $C_p$ | $T$ | $C_p$ |
|---|---|---|---|---|---|---|---|---|---|---|---|
| K | $J \cdot K^{-1} \cdot mol^{-1}$ | K | $J \cdot K^{-1} \cdot mol^{-1}$ | K | $J \cdot K^{-1} \cdot mol^{-1}$ | K | $J \cdot K^{-1} \cdot mol^{-1}$ | K | $J \cdot K^{-1} \cdot mol^{-1}$ | K | $J \cdot K^{-1} \cdot mol^{-1}$ |
| 12.39 | 11.05 | 50.31 | 109.74 | 103.75 | 213.36 | 176.95 | 326.52 | 250.96 | 457.02 | 301.47 | 662.23 |
| 13.45 | 13.82 | 51.79 | 113.29 | 106.76 | 217.88 | 179.88 | 330.97 | 253.79 | 461.16 | 303.40 | 681.19 |
| 14.75 | 17.10 | 53.37 | 116.71 | 109.83 | 222.61 | 182.78 | 335.51 | 256.78 | 468.58 | 305.41 | 679.11 |
| 16.16 | 20.67 | 55.25 | 121.11 | 112.84 | 227.26 | 185.67 | 339.96 | 259.74 | 476.27 | 307.42 | 671.57 |
| 17.60 | 23.93 | 57.39 | 126.11 | 115.80 | 231.89 | 188.54 | 344.67 | 262.68 | 484.46 | 309.43 | 688.64 |
| 19.11 | 27.88 | 59.42 | 130.34 | 118.71 | 236.48 | 191.39 | 349.01 | 265.60 | 502.35 | 313.49 | 701.76 |
| 20.39 | 31.03 | 61.46 | 135.01 | 121.57 | 241.07 | 194.22 | 353.50 | 268.05 | 547.35 | 315.46 | 723.73 |
| 21.71 | 34.31 | 63.58 | 139.46 | 124.39 | 245.74 | 197.03 | 356.15 | 270.02 | 606.72 | 317.42 | 708.62 |
| 23.21 | 38.40 | 65.71 | 143.97 | 127.18 | 250.08 | 199.93 | 361.90 | 271.91 | 695.70 | 319.40 | 699.00 |
| 24.74 | 42.66 | 67.86 | 148.32 | 129.92 | 254.52 | 202.90 | 366.93 | 273.70 | 820.27 | 321.38 | 693.40 |
| 26.31 | 47.20 | 70.03 | 152.75 | 132.64 | 258.89 | 205.86 | 370.26 | 275.37 | 991.51 | 323.36 | 681.25 |
| 27.90 | 51.69 | 72.22 | 157.57 | 135.32 | 263.03 | 208.79 | 375.35 | 276.89 | 1197.3 | 325.35 | 690.00 |
| 29.56 | 56.20 | 74.41 | 161.89 | 137.97 | 267.28 | 211.71 | 379.89 | 278.29 | 1418.2 | 327.34 | 685.18 |
| 31.35 | 61.10 | 76.54 | 166.16 | 140.59 | 271.52 | 214.61 | 384.82 | 279.57 | 1624.9 | 329.33 | 679.06 |
| 33.17 | 66.04 | 78.60 | 170.30 | 143.19 | 275.24 | 217.50 | 389.73 | 280.79 | 1730.1 | 331.33 | 673.06 |
| 34.90 | 70.98 | 80.60 | 174.05 | 145.77 | 279.41 | 220.37 | 394.59 | 282.01 | 1567.4 | 333.33 | 666.13 |
| 36.56 | 75.01 | 82.56 | 177.72 | 148.32 | 283.47 | 223.22 | 400.00 | 283.36 | 1235.9 | 335.34 | 658.10 |
| 38.22 | 79.52 | 84.47 | 181.23 | 150.85 | 287.46 | 226.05 | 405.66 | 284.87 | 873.62 | 337.35 | 651.01 |
| 39.89 | 83.81 | 86.35 | 184.59 | 153.35 | 291.30 | 228.88 | 410.81 | 286.61 | 742.83 | 339.37 | 644.61 |
| 41.44 | 87.88 | 88.18 | 187.74 | 156.05 | 295.48 | 231.68 | 415.55 | 288.43 | 686.48 | 341.40 | 637.14 |
| 42.89 | 91.64 | 89.98 | 190.91 | 158.98 | 299.15 | 234.48 | 421.90 | 290.28 | 664.69 | 343.43 | 632.38 |
| 44.25 | 95.35 | 91.75 | 194.17 | 161.99 | 304.50 | 237.26 | 427.12 | 292.15 | 658.36 | 345.46 | 629.92 |
| 45.55 | 98.37 | 93.48 | 197.09 | 165.03 | 309.38 | 240.02 | 432.60 | 294.01 | 660.93 | 347.50 | 629.84 |
| 46.78 | 101.50 | 95.29 | 199.50 | 168.05 | 313.82 | 242.77 | 439.08 | 295.87 | 657.86 | 349.53 | 629.69 |
| 47.96 | 104.31 | 97.76 | 203.91 | 171.04 | 317.27 | 245.51 | 445.11 | 297.74 | 653.67 | | |
| 49.09 | 106.93 | 100.79 | 208.77 | 174.01 | 321.92 | 248.24 | 451.01 | 299.60 | 656.76 | | |

Table 2. Molar Heat Capacities of the Metastable LS and the Undercooled HS Phases of the Spin Crossover Complex $[Fe(2\text{-pic})_3]Cl_2 \cdot H_2O$ (Specimen A, Relative Molar Mass 483.22)

| $T$ | $C_p$ | $T$ | $C_p$ | $T$ | $C_p$ | $T$ | $C_p$ | $T$ | $C_p$ | $T$ | $C_p$ |
|---|---|---|---|---|---|---|---|---|---|---|---|
| K | $J \cdot K^{-1} \cdot mol^{-1}$ | K | $J \cdot K^{-1} \cdot mol^{-1}$ | K | $J \cdot K^{-1} \cdot mol^{-1}$ | K | $J \cdot K^{-1} \cdot mol^{-1}$ | K | $J \cdot K^{-1} \cdot mol^{-1}$ | K | $J \cdot K^{-1} \cdot mol^{-1}$ |
| 12.97 | 12.90 | 79.06 | 172.43 | 123.45 | 245.18 | 180.21 | 340.11 | 230.38 | 441.94 | 294.81 | 539.47 |
| 14.60 | 17.09 | 80.85 | 175.52 | 124.89 | 247.80 | 181.99 | 343.52 | 232.43 | 443.63 | 296.51 | 543.44 |
| 16.73 | 22.29 | 82.29 | 178.39 | 126.33 | 250.27 | 183.76 | 345.95 | 234.46 | 446.81 | 298.37 | 548.22 |
| 18.39 | 26.29 | 83.71 | 180.88 | 127.75 | 252.01 | 185.52 | 350.20 | 236.50 | 449.80 | 300.22 | 551.10 |
| 20.01 | 30.43 | 85.10 | 183.04 | 129.17 | 254.87 | 187.27 | 354.78 | 238.52 | 452.68 | 302.07 | 555.19 |
| 21.74 | 35.02 | 86.47 | 185.38 | 130.58 | 256.35 | 189.02 | 357.49 | 240.54 | 455.50 | 303.91 | 558.19 |
| 23.54 | 40.88 | 87.82 | 188.06 | 131.98 | 258.65 | 190.76 | 362.38 | 242.56 | 458.18 | 305.74 | 560.47 |
| 25.49 | 45.47 | 89.15 | 190.34 | 133.37 | 261.11 | 192.49 | 365.81 | 244.56 | 461.34 | 307.58 | 563.05 |
| 27.61 | 51.51 | 90.46 | 191.87 | 134.75 | 264.29 | 194.21 | 369.54 | 246.57 | 464.33 | 309.41 | 565.45 |
| 29.75 | 57.31 | 91.76 | 195.03 | 136.12 | 266.60 | 195.92 | 372.63 | 248.56 | 467.32 | 311.24 | 567.02 |
| 32.10 | 63.77 | 93.04 | 196.61 | 137.49 | 268.60 | 197.90 | 377.28 | 250.52 | 469.49 | 313.06 | 571.33 |
| 34.21 | 69.61 | 94.30 | 198.94 | 138.85 | 270.11 | 198.93 | 380.39 | 252.51 | 472.67 | 314.88 | 573.79 |
| 36.20 | 74.98 | 95.56 | 201.09 | 140.53 | 273.92 | 200.62 | 385.97 | 254.49 | 475.37 | 316.69 | 576.55 |
| 38.07 | 80.09 | 96.79 | 203.15 | 142.54 | 277.21 | 202.96 | 392.08 | 256.47 | 478.22 | 318.51 | 578.97 |
| 39.96 | 84.83 | 98.02 | 205.11 | 144.54 | 280.34 | 205.28 | 398.71 | 258.44 | 481.13 | 320.31 | 582.59 |
| 41.85 | 89.65 | 99.23 | 207.72 | 146.52 | 284.17 | | | 260.40 | 484.27 | 322.11 | 587.51 |
| 43.74 | 94.38 | 100.43 | 208.88 | 148.49 | 286.89 | 202.22 | 414.78 | 262.36 | 487.09 | 323.91 | 593.07 |
| 45.61 | 98.99 | 101.62 | 211.41 | 150.44 | 289.91 | 203.42 | 415.04 | 264.31 | 490.17 | 325.69 | 598.34 |
| 47.48 | 103.45 | 102.80 | 212.02 | 152.38 | 293.41 | 204.63 | 415.44 | 266.26 | 493.67 | 327.47 | 601.35 |
| 49.50 | 108.20 | 103.96 | 213.84 | 154.31 | 296.49 | 205.83 | 415.98 | 268.21 | 496.27 | 329.25 | 605.53 |
| 51.40 | 112.50 | 105.12 | 216.15 | 156.23 | 299.74 | 207.03 | 417.30 | 270.14 | 498.99 | 331.41 | 608.76 |
| 53.39 | 117.21 | 106.27 | 218.42 | 158.14 | 302.75 | 208.17 | 418.61 | 272.08 | 501.81 | 333.96 | 611.27 |
| 55.48 | 121.98 | 107.41 | 219.66 | 160.03 | 305.55 | 210.12 | 419.84 | 274.00 | 504.29 | 336.51 | 610.11 |
| 57.45 | 126.54 | 108.54 | 221.05 | 161.91 | 309.13 | 212.06 | 421.47 | 275.92 | 507.77 | 339.06 | 611.33 |
| 59.51 | 131.15 | 109.89 | 223.36 | 163.79 | 311.60 | 214.00 | 423.17 | 277.84 | 511.06 | 341.61 | 612.19 |
| 61.87 | 136.20 | 111.45 | 225.61 | 165.65 | 314.41 | 215.94 | 424.95 | 279.75 | 513.73 | 344.15 | 615.05 |
| 64.34 | 141.61 | 113.00 | 228.06 | 167.50 | 317.32 | 217.86 | 427.00 | 281.66 | 517.15 | 346.69 | 617.60 |
| 66.68 | 146.97 | 114.53 | 230.69 | 169.34 | 320.60 | 219.79 | 429.51 | 283.56 | 520.71 | 349.23 | 621.00 |
| 68.93 | 152.06 | 116.04 | 233.22 | 171.18 | 323.71 | 221.70 | 430.99 | 285.45 | 523.51 | | |
| 71.09 | 156.90 | 117.55 | 235.49 | 173.00 | 326.67 | 222.94 | 432.71 | 287.34 | 527.05 | | |
| 73.17 | 161.29 | 119.04 | 237.95 | 174.81 | 330.09 | 224.69 | 434.89 | 289.22 | 530.17 | | |
| 75.19 | 165.24 | 120.52 | 240.01 | 176.62 | 332.99 | 226.43 | 436.78 | 291.10 | 534.24 | | |
| 77.15 | 168.95 | 121.99 | 242.59 | 178.42 | 336.45 | 228.33 | 439.22 | 292.96 | 537.84 | | |

impossible to measure the heat capacity in the cooling direction by using a common adiabatic calorimeter, we measured $C_p$ values by repeating the usual $C_p$ measurement in the heating direction after cooling down of the sample by 5–10 K. With this method, we succeeded in the $C_p$ measurement from 200 K to 350 K. The results are shown by solid circles in Fig. 3. As was expected, the transition peak at 280.79 K completely vanished, while a very small hump was still observed at temperatures above 300 K, as seen in Fig. 3. The heat capacity measurement could not be continued below 200 K because the heat evolution began to be observed. This temperature just corresponds to the $T_c(\downarrow)$ determined by the $^{57}$Fe Mössbauer spectroscopy and the preliminary DTA measurement, implying that this heat evolution originates from the phase transition from the HS state to the metastable LS state just corresponding to that observed in the initial cooling process.

**Determination of the Absolute Enthalpy of the Metastable Phase, Referred to the Stable Phase, by Using Specimen B.** Because of the unexpected stabilization around 200 K, the heat capacity data around the phase transition from the metastable LS phase to the stable LS phase could not be measured. A specimen that had once experienced this stabilization did not show the same thermal properties as those of the virginal sample. Consequently, we lacked not only the $C_p$ data but also some fundamental thermodynamic information on this system such as the transition enthalpy between these phases and the enthalpy relation between the metastable and the stable phases. In order to fill these deficits, another measurement was made by using freshly prepared specimen B.

First, in order to determine the enthalpy difference between the metastable LS phase and the undercooled HS phase, the heat capacities were measured by "continuous heating mode" with a constant current. According to this method, the enthalpy change between the initial state and the final state can be determined provided the temperatures of the initial and the final states are precisely determined. However the heat capacity value itself is not so accurate because of the heat evolution. The estimated $C_p$ data are plotted in Fig. 4 together with those for specimen A and are listed in Table 3. The heating rate was gradually varied from $\sim$8 K h$^{-1}$ at 150 K to $\sim$5 K h$^{-1}$ at 300 K depending on the total $C_p$ value of the calorimeter cell containing the sample. Two peaks were observed, at 228 K ($T_{trs2}$) and at 265 K ($T_{trs3}$). The $C_p$ values around the first peak would be small in comparison to the intrinsic values, owing to the heat evolution from the sample, because the stabilization also occurred during the heating. The peak at 228 K obviously corresponds to the transition from the metastable LS to the undercooled HS phase, while that at 265 K is clearly different from the transition peak at 281 K observed for the specimen A. Since the $C_p$ values above 270 K for specimen B are almost the same as those of the undercooled HS phase of specimen A, the phase of the specimen B below 270 K seemed to be in a different low-temperature phase. These facts indicate the existence of another metastable phase (labeled by J in Fig. 12 presented later). The spin state of this new phase is probably low-spin, although there are neither magnetic nor $^{57}$Fe Mössbauer data. Since no anomaly was observed around 280 K in the $C_p$ data, one can anticipate that none of the sample was stabilized to the stable LS state. In what follows, we shall designate the two low-temperature phases appearing below 200 K and 265 K as the metastable LS phases (1) and (2), respectively.

One of the purposes of the present calorimetric measurement for the specimen B was to determine the enthalpy relationship between the metastable LS state (1) and the undercooled HS state. Figure 5 schematically illustrates the enthalpy against temperature relation. It should be remarked here that the present measurement has been done under adiabatic conditions and moreover that enthalpy is a state function. Therefore, the enthalpy difference between the initial and the final states does not depend on the path connecting the two states. Let's consider now the present continuous heating for the specimen B. The initial state at temperature $T_i$ is a state in the metastable LS phase (1), and the final state at temperature $T_f$ is a state in the undercooled HS phase. The enthalpy of the calorimeter cell at $T_i$ is the sum of the specimen $H$[msLS(1),$T_i$] and the sample con-

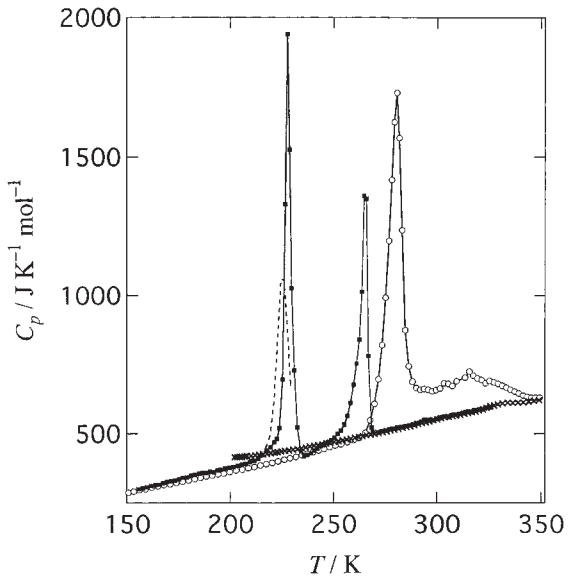


Fig. 4. Plot of molar heat capacity of $[Fe(2\text{-pic})_3]Cl_2 \cdot H_2O$ (specimen B) vs temperature determined by the continuous heating method (solid square). The data for specimen A are also shown by open circle (stable phases), cross (the undercooled HS phase), and dotted curve (the metastable LS phase (1)).

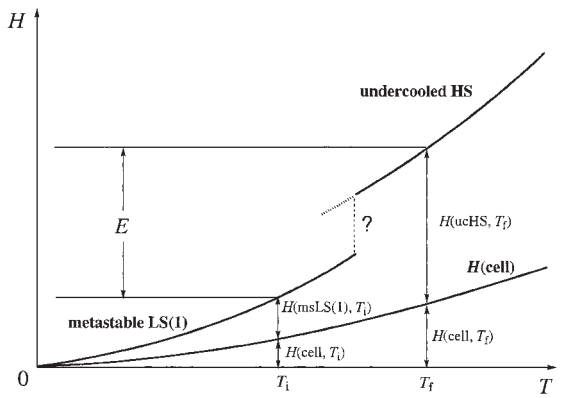


Fig. 5. Schematic representation of the enthalpy vs temperature relationship for the calorimeter cell containing the sample.

Table 3. Molar Heat Capacities of the Spin Crossover Complex $[Fe(2\text{-pic})_3]Cl_2 \cdot H_2O$ (Relative Molar Mass 483.22) Obtained by the Continuous Heating Method for the Metastable LS Phase of Specimens A and B

| $T$ | $C_p$ | $T$ | $C_p$ | $T$ | $C_p$ | $T$ | $C_p$ | $T$ | $C_p$ | $T$ | $C_p$ |
|---|---|---|---|---|---|---|---|---|---|---|---|
| K | $J \cdot K^{-1} \cdot mol^{-1}$ | K | $J \cdot K^{-1} \cdot mol^{-1}$ | K | $J \cdot K^{-1} \cdot mol^{-1}$ | K | $J \cdot K^{-1} \cdot mol^{-1}$ | K | $J \cdot K^{-1} \cdot mol^{-1}$ | K | $J \cdot K^{-1} \cdot mol^{-1}$ |
| | | 201.57 | 379.27 | 272.83 | 505.79 | 180.31 | 333.20 | 254.46 | 467.90 | 306.15 | 657.18 |
| Specimen A | | 203.62 | 384.53 | 274.28 | 508.81 | 182.05 | 340.83 | 255.95 | 468.60 | 307.13 | 660.76 |
| | | 205.66 | 386.62 | 275.72 | 511.13 | 183.78 | 339.27 | 257.45 | 473.54 | 308.11 | 658.78 |
| 200.94 | 383.49 | 207.70 | 390.87 | 277.16 | 514.13 | 185.51 | 342.02 | 258.93 | 477.54 | 309.09 | 661.92 |
| 203.03 | 388.13 | 209.72 | 397.04 | 278.59 | 516.66 | 187.23 | 344.01 | 260.41 | 485.02 | 310.06 | 665.26 |
| 205.11 | 394.19 | 211.73 | 402.52 | 280.03 | 517.03 | 188.95 | 348.65 | 261.88 | 494.36 | 311.04 | 663.21 |
| 207.18 | 399.09 | 213.73 | 409.35 | 281.46 | 522.13 | 190.65 | 350.41 | 263.34 | 510.89 | 312.01 | 665.90 |
| 209.23 | 407.05 | 215.72 | 423.35 | 282.88 | 522.79 | 192.36 | 351.67 | 264.78 | 534.35 | 312.98 | 667.49 |
| 211.27 | 412.45 | 217.67 | 438.99 | 284.31 | 525.19 | 194.05 | 355.02 | 266.19 | 563.68 | 313.95 | 667.36 |
| 213.30 | 420.62 | 219.61 | 450.75 | 285.73 | 526.23 | 195.74 | 357.49 | 267.58 | 604.65 | 314.92 | 667.51 |
| 215.30 | 434.20 | 221.53 | 469.55 | 287.15 | 529.67 | 197.42 | 361.68 | 268.93 | 653.15 | 315.89 | 665.46 |
| 217.29 | 453.85 | 222.66 | 480.73 | 288.57 | 531.89 | 199.10 | 361.20 | 270.24 | 699.68 | 316.87 | 666.17 |
| 219.23 | 498.35 | 223.78 | 519.19 | 289.98 | 536.52 | 200.77 | 366.32 | 271.51 | 750.43 | 317.83 | 668.43 |
| 221.08 | 618.98 | 225.30 | 694.04 | 291.39 | 537.47 | 202.43 | 369.05 | 272.75 | 809.84 | 318.80 | 665.04 |
| 222.75 | 857.83 | 226.55 | 1331.1 | 292.79 | 544.56 | 204.09 | 366.36 | 273.95 | 884.25 | 319.78 | 662.32 |
| 224.24 | 1062.6 | 227.49 | 1941.5 | 294.18 | 550.64 | 205.75 | 373.07 | 275.09 | 1004.6 | 320.75 | 660.75 |
| 225.66 | 1056.5 | 228.40 | 1525.8 | 295.57 | 549.41 | 207.39 | 378.58 | 276.16 | 1133.3 | 321.72 | 659.51 |
| 227.14 | 890.30 | 229.50 | 1025.6 | 296.96 | 550.33 | 209.03 | 377.89 | 277.17 | 1302.0 | 322.69 | 657.13 |
| 228.76 | 676.54 | 230.80 | 727.77 | 298.36 | 549.04 | 210.67 | 381.49 | 278.11 | 1467.3 | 323.67 | 653.41 |
| | | 232.30 | 521.50 | 299.75 | 551.68 | 212.30 | 380.64 | 278.99 | 1599.2 | 324.64 | 652.38 |
| Specimen B | | 233.94 | 436.70 | 301.14 | 555.65 | 213.93 | 387.72 | 279.86 | 1619.9 | 325.62 | 646.91 |
| | | 235.62 | 419.00 | 302.52 | 559.47 | 215.55 | 388.58 | 280.72 | 1539.7 | 326.59 | 644.47 |
| 155.68 | 299.60 | 237.32 | 421.86 | 303.91 | 561.10 | 217.16 | 390.93 | 281.63 | 1407.2 | 327.57 | 641.21 |
| 157.70 | 303.20 | 239.00 | 428.56 | 305.29 | 560.36 | 218.77 | 394.41 | 282.59 | 1256.9 | 328.56 | 639.05 |
| 159.71 | 307.07 | 240.68 | 438.45 | 306.67 | 564.13 | 220.38 | 396.63 | 283.60 | 1128.9 | 329.54 | 636.39 |
| 161.71 | 310.68 | 242.34 | 446.93 | 308.05 | 567.13 | 221.98 | 396.85 | 284.68 | 992.11 | 330.52 | 633.09 |
| 163.69 | 314.58 | 244.00 | 454.47 | 309.42 | 568.73 | 223.57 | 402.35 | 285.82 | 885.60 | 331.51 | 628.03 |
| 165.66 | 316.06 | 245.64 | 461.19 | 310.80 | 570.24 | 225.16 | 407.68 | 287.02 | 780.30 | 332.49 | 625.98 |
| 167.62 | 321.68 | 247.28 | 470.07 | 312.17 | 572.06 | 226.75 | 406.31 | 288.27 | 713.45 | 333.48 | 623.48 |
| 169.56 | 324.15 | 248.90 | 476.45 | 313.53 | 577.22 | 228.32 | 414.98 | 289.56 | 676.28 | 334.47 | 620.74 |
| 171.50 | 327.96 | 250.52 | 484.91 | 314.90 | 580.11 | 229.90 | 415.45 | 290.31 | 665.33 | 335.46 | 617.43 |
| 173.43 | 330.74 | 252.12 | 498.65 | 316.26 | 578.11 | 231.47 | 415.29 | 291.29 | 645.58 | 336.45 | 616.01 |
| 175.34 | 335.13 | 253.71 | 511.24 | 317.62 | 584.31 | 233.03 | 417.69 | 292.28 | 639.19 | 337.44 | 615.39 |
| 177.24 | 340.49 | 255.28 | 532.07 | 318.98 | 584.83 | 234.59 | 425.39 | 293.27 | 634.21 | 338.44 | 610.23 |
| 179.14 | 342.50 | 256.83 | 562.88 | 320.33 | 588.18 | 236.15 | 426.93 | 294.26 | 634.23 | 339.43 | 611.90 |
| 181.02 | 348.44 | 258.34 | 610.66 | 321.68 | 588.09 | 237.70 | 425.49 | 295.26 | 626.66 | 340.42 | 609.50 |
| 182.89 | 350.94 | 259.79 | 675.76 | 323.03 | 590.33 | 239.24 | 437.11 | 296.25 | 628.96 | 341.42 | 609.76 |
| 184.75 | 355.56 | 261.20 | 752.14 | 324.38 | 594.76 | 240.78 | 436.10 | 297.25 | 625.60 | 342.41 | 607.23 |
| 186.61 | 357.80 | 262.54 | 839.21 | 325.72 | 593.78 | 242.32 | 436.50 | 298.25 | 628.31 | 343.40 | 607.42 |
| 188.45 | 357.71 | 263.79 | 1013.0 | | | 243.85 | 443.74 | 299.25 | 628.61 | 344.40 | 607.01 |
| 190.30 | 361.90 | 264.91 | 1360.0 | 169.67 | 317.40 | 245.38 | 445.69 | 300.24 | 635.88 | 345.39 | 609.32 |
| 192.13 | 360.02 | 265.94 | 1349.8 | 171.46 | 319.65 | 246.90 | 447.95 | 301.23 | 638.58 | 346.38 | 604.44 |
| 193.96 | 367.70 | 267.14 | 779.52 | 173.25 | 322.85 | 248.42 | 450.21 | 302.22 | 645.50 | 347.37 | 610.30 |
| 195.35 | 370.31 | 268.59 | 521.59 | 175.02 | 324.13 | 249.94 | 451.78 | 303.21 | 646.60 | 348.36 | 611.03 |
| 197.43 | 374.51 | 269.21 | 506.10 | 176.79 | 329.11 | 251.45 | 462.53 | 304.19 | 652.01 | 349.35 | 608.27 |
| 199.51 | 376.34 | 272.02 | 502.63 | 178.55 | 327.87 | 252.96 | 454.87 | 305.17 | 653.97 | | |

tainer $H(\text{cell},T_i)$ and that at $T_f$ is $H(\text{ucHS},T_f) + H(\text{cell},T_f)$. The enthalpy difference between the two temperature just corresponds to the Joule-energy $E$ supplied to the calorimeter cell by the electric heater attached to the cell, because the calorimetry has been done under adiabatic condition. In the present case, although a part of the specimen was stabilized to the newly discovered metastable LS phase (2), the whole specimen was finally transformed to the undercooled HS phase through the phase transition at 265 K. Therefore, the total input energy $E$ can be regarded as being used for the rise in temperature of the calorimeter cell containing the sample from $T_i$ in the metastable LS phase (1) to $T_f$ in the undercooled HS phase. As is easily recognized from Fig. 5, the energy relation can be given in terms of molar enthalpy $H_m$ as follows:

$$H_m[\text{msLS}(1),T_i] + fH(\text{cell},T_i) + fE = H_m(\text{ucHS},T_f) + fH(\text{cell},T_f), \quad (2)$$

where $f$ is the mole factor ($= 1/0.00927286 = 107.842$) to reduce the experimental value to molar quantity. The molar enthalpy change of the sample from the initial to the final temperature can be derived as

$$H_m(\text{ucHS},T_f) - H_m[\text{msLS}(1),T_i] = f[E + H(\text{cell},T_i) - H(\text{cell},T_f)]. \quad (3)$$

To determine the molar enthalpy change of the sample, we

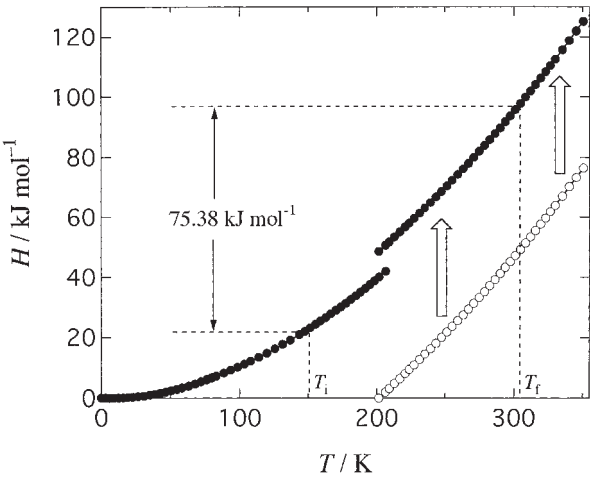


Fig. 6. Plot of how to correlate the molar enthalpies of the metastable LS phase (1) and the undercooled HS phase of $[Fe(2\text{-pic})_3]Cl_2 \cdot H_2O$. The open circles indicate the molar enthalpy values of the undercooled HS phase referred to 201.615 K as the origin of the enthalpy. The large arrows indicate that the enthalpy values in the temperature range (350 K > $T$ > 201 K) are parallel shifted upward by 75.38 kJ mol$^{-1}$.

adopted the values of $T_i = 149.221$ K, $T_f = 305.086$ K, and $E = 2218.64$ J. The enthalpy change from $T_i$ to $T_f$ was determined as

$$H_m(\text{ucHS}, T_f) - H_m[\text{msLS}(1), T_i] = 75.38 \text{ kJ mol}^{-1}. \quad (4)$$

We adopted this value to the case of specimen A and obtained the enthalpy relationship between the metastable LS phase (1) and the undercooled HS phase over the whole temperature region studied here (see Fig. 6). In this calculation, the $H_m$ values for the metastable LS phase (1) below 13 K were evaluated from the $C_p$ values estimated by the effective frequency distribution method (see below).[14] At the present stage, the molar enthalpies of the metastable LS phase (1) and the undercooled HS phase are not absolute values, because the origin of the enthalpy at 0 K has tentatively been referred to the metastable LS phase (1).

The next step is, therefore, to determine the enthalpy relationship between the metastable LS phase (1) and the stable LS phase on the basis of the spontaneous stabilization from the former to the latter occurring around at 200 K. The enthalpy vs temperature relationship is schematically shown in Fig. 7. Let's consider now that the specimen in the metastable LS phase (1) happens to undergo the stabilization at $T_i$. Since the present calorimetry has been done under adiabatic conditions, the total enthalpy of the calorimeter cell and the specimen remains constant before and after the stabilization. The final temperature eventually reached is designated as $T_f$ in Fig. 7. The simple way to establish the enthalpy relation is to determine $T_i$ and $T_f$ precisely. However, it is experimentally not so easy to determine accurately the initial temperature $T_i$. We then started the measurement from $T_I$, a temperature fairly lower than $T_i$, by supplying the Joule-energy to the calorimeter. When the input energy amounted to $E_1$, the spontaneous stabilization took place around $T_i$ and the temperature of the calorimeter cell became $T_f$. In order to confirm the complete stabilization, addi-

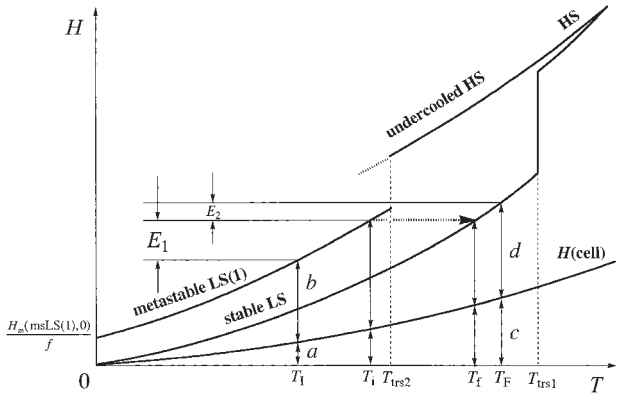


Fig. 7. Schematic drawing of the enthalpy vs temperature relationship for the calorimeter cell containing the sample.

tional Joule-energy $E_2$ was supplied to the calorimeter and thereby the final temperature became $T_F$. In Fig. 7, the enthalpy balance is realized as $a + b + E_1 + E_2 = c + d$, where $a = H(\text{cell}, T_I)$, $b = H[\text{msLS}(1), T_I] + H_m[\text{msLS}(1), 0]/f$, $c = H(\text{cell}, T_F)$, and $d = H(\text{sLS}, T_F)$. It should be remarked here that $H[\text{msLS}(1), T_I]$ is the experimental enthalpy having its origin at 0 K, while $H_m[\text{msLS}(1), 0]$ is the molar enthalpy at 0 K possessed by the metastable LS phase (1).

In accordance with the previous discussion, the experimental enthalpies were reduced to the molar quantities by use of the mole factor $f$. The only unknown quantity is the molar enthalpy of the metastable LS phase (1) at 0 K, $H_m[\text{msLS}(1), 0]$. This value is determined by the following equation:

$$H_m[\text{msLS}(1), 0] = H_m(\text{sLS}, T_F) - H_m[\text{msLS}(1), T_I] - H_m(\text{sLS}, T_I) + f[H(\text{cell}, T_F) - H(\text{cell}, T_I) - E_1 - E_2]. \quad (5)$$

In the present calculation, we adopted the values of $T_I = 149.645$ K, $T_F = 228.208$ K, $E_1 = 814.830$ J, and $E_2 = 105.481$ J, and obtained the final result:

$$H_m[\text{msLS}(1), 0] = (6.0 \pm 0.4) \text{ kJ mol}^{-1}. \quad (6)$$

The main part of the error bound originates in the long experimental time during which a small, uncorrectable heat leak is involved.

The resultant enthalpy relation between the metastable LS phase (1) and the undercooled HS phase is compared in Fig. 8(a) with the molar enthalpy of the stable LS and HS phases. These two sets of data should coincide with each other at 350 K, the highest temperature studied here, where the specimen is likewise in the HS phase for both sets of data. In reality there existed a small discrepancy of 0.82 kJ mol$^{-1}$, corresponding to 0.63% of the molar enthalpy. However, if we take into account the fact that the data have been independently determined, the agreement is excellent.

On the other hand, the molar entropies of various phases given in Fig. 8(b) were obtained by a slightly different manner. The molar entropy of the undercooled HS state was determined by assuming that the entropy values of the undercooled HS and the HS states should coincide at 350 K. As described below, the entropy of the metastable LS phase (1) referred to the undercooled HS state was determined so as to have a vertical jump

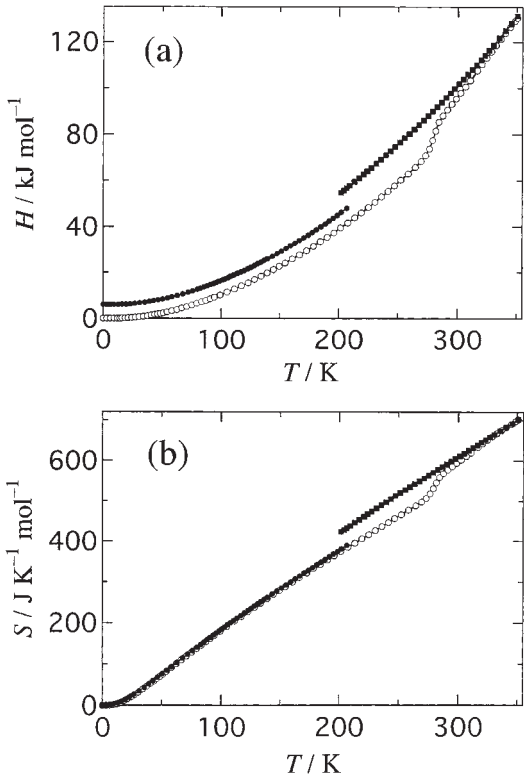


Fig. 8. Molar enthalpy (a) and entropy (b) of $[Fe(2\text{-pic})_3]Cl_2 \cdot H_2O$. Open circles: The values for the stable phases, solid circles: the metastable LS phase (1), solid squares: the undercooled HS phase.

41.58 J K$^{-1}$ mol$^{-1}$ at 206.4 K. This entropy jump was determined from a relation $\Delta S = \Delta H/T$, where $\Delta H = 8.58$ kJ mol$^{-1}$ from Fig. 8(a). The reason for the adopted temperature 206.4 K was as follows: (i) This temperature is close to the phase transition from the metastable LS phase (1) to the undercooled HS phase, and (ii) at this temperature the entropy data of both the phases are available. This treatment brought about a small residual entropy of +0.75 J K$^{-1}$ mol$^{-1}$ at 0 K for the metastable LS phase (1). However, as this value is extremely small in comparison to the value in usual glass forming materials, it can be regarded as substantially zero within the experimental errors. The present calorimetric study confirmed that the metastable LS phase (1) has no residual entropy and hence obeys the third law of thermodynamics.

In order to examine the sample dependence of the phase transition, we measured the heat capacity from the stable LS to the HS phases for specimen B by the continuous heating mode. The data are compared in Fig. 9 with the $C_p$ data for specimen A determined by the usual intermittent heating method. Although the measuring methods were different, the two sets of data agreed well.

## Discussion

For determination of the excess heat capacities due to the spin crossover phenomenon, the normal heat capacity curve was determined by the effective frequency distribution method.[14] Because of the lack of the $C_p$ data in the vicinity of the phase transition for the metastable LS phase (1), this calculation was applied only to the stable LS phase (sLS). For determination of the $C_{lat}$(sLS), we used 87 $C_p$ values in the 12–200 K temperature range. The 'best' $C_{lat}$(sLS) curve determined by the least-squares fitting is reproduced in Fig. 3. On the other hand, since the spin crossover phase transition at 280.79 K is principally of first order, there may be a discontinuity at $T_{trs1}$, a jump of the lattice heat capacities from the LS to the HS phase. Therefore the extrapolation of the $C_{lat}$ curve estimated for the stable LS state cannot be used for the HS phase. We must determine the lattice heat capacities for the HS phase, $C_{lat}$(HS). However, it is difficult to independently determine the lattice heat capacities for the phase transition peak and the broad hump. Therefore, we adopted the $C_p$ data for the undercooled HS phase as the normal heat capacity curve at temperatures $T_{trs1} < T < \sim 350$ K. The $C_{lat}$(HS) curve was estimated by a least squares fitting of the $C_p$ data in the temperature ranges 200 K $< T <$ 292 K, 295 K $< T <$ 320 K, and 340 K $< T <$ 350 K, excluding small humps. We used a polynomial function of temperature, $aT^3 + bT^2 + cT + d$, to fit the $C_p$ data. The 'best' fit $C_{lat}$ curve thus determined is represented by the following equation and reproduced in Fig. 3 by the broken line:

$$C_{lat}/\mathrm{J\,K^{-1}\,mol^{-1}} = 1107 - 9.360(T/\mathrm{K})3 + 0.003830(T/\mathrm{K})^2 - 0.00004431(T/\mathrm{K})^3. \quad (7)$$

The difference between the observed and the normal heat capacities shown in Fig. 10 corresponds to the excess heat capacity, $\Delta C_p$, due to the spin crossover phenomenon from the stable LS to the HS phase. The excess enthalpy, $\Delta_{trs}H$, and entropy, $\Delta_{trs}S$, arising from the spin crossover phenomenon were determined by integration of $\Delta C_p$ with respect to $T$ and to $\ln T$, respectively. The temperature dependence of the $\Delta_{trs}H$ and $\Delta_{trs}S$ are plotted in Fig. 11. The total enthalpy and entropy gained at the spin crossover transition and the hump are $\Delta_{trs}H = 17.5$ kJ mol$^{-1}$ and $\Delta_{trs}S = 61.0$ J K$^{-1}$ mol$^{-1}$, respectively.

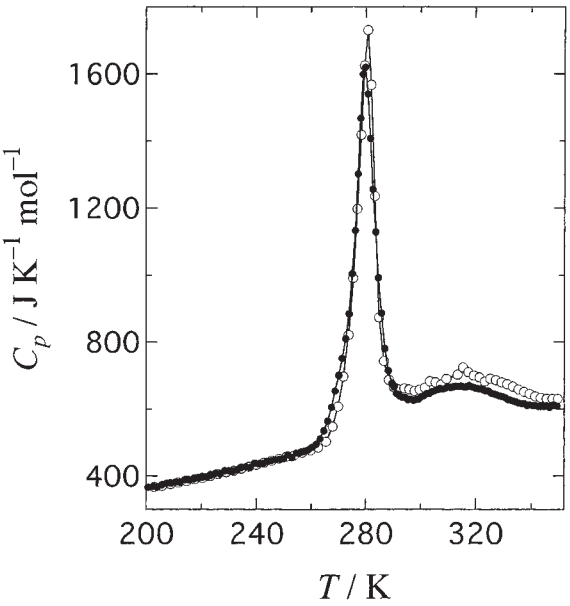


Fig. 9. Molar heat capacity of $[Fe(2\text{-pic})_3]Cl_2 \cdot H_2O$ around the spin crossover phase transition. Open circles: Data for specimen A determined by usual intermittent heating method. Solid circles: Data for specimen B determined by the continuous heating method.

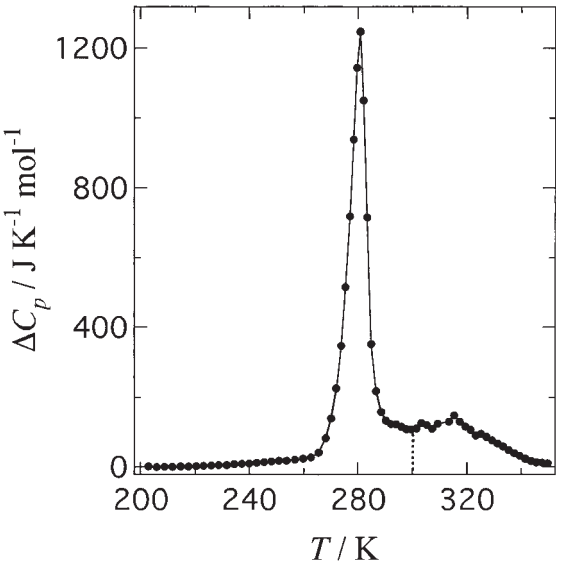


Fig. 10. Excess heat capacity of $[Fe(2\text{-pic})_3]Cl_2 \cdot H_2O$ (specimen A) due to the spin crossover phenomenon. Vertical broken line is a boundary tentatively dividing the contributions from the spin crossover phase transition and the broad heat capacity anomaly.

The origin of the hump should be discussed here. As shown by the previous $^{57}$Fe Mössbauer study,[9] the spin crossover phase transition from the stable LS to the HS seems to be terminated at ~300 K. Therefore, it is very likely that only the main transition peak corresponds to the 'spin transition' and that the subsequent hump corresponds to a different phase transition. Since the hump was confirmed to have a first-order character, we suggest that the origin of the hump is somewhat of a gradual structure change, although there is no evidence to support this suggestion at the present stage. It should be emphasized that the origin of the hump can never be dehydration of this complex, because the hump is always observed together with the transition peak at 280 K but is not observed in the first heating for freshly prepared sample from room temperature to 350 K or even in a sample kept in the undercooled HS phase at room temperature for a few days. If we distribute the enthalpy and entropy gains between the main phase transition and the hump by tentatively dividing at 300 K (broken lines in Fig. 10), we get the following result: $\Delta_{trs}H = 13.1$ kJ mol$^{-1}$ and $\Delta_{trs}S = 47.0$ J K$^{-1}$ mol$^{-1}$ for the main phase transition and $\Delta_{trs}H = 4.4$ kJ mol$^{-1}$ and $\Delta_{trs}S = 14.0$ J K$^{-1}$ mol$^{-1}$ for the broad anomaly. In any case, the entropy gain is much larger than the value expected for the change in the spin manifold of a Fe(II) complex, $R\ln 5$ (= 13.4 J K$^{-1}$ mol$^{-1}$). As there is no crystal structure determination of this complex, one cannot exclude the possibility that the excess entropy gain includes the contribution from the disordering of the water solvate molecule. On the other hand, if there is no order–disorder transition, the remaining entropy gain 33.6 J K$^{-1}$ mol$^{-1}$ may be attributed to the change in the internal vibrations.[5] It should be remarked that this value is similar to those previously reported for the vibrational entropy change in the spin crossover phenomenon: 28.24 J K$^{-1}$ mol$^{-1}$ for $[Fe(2\text{-pic})_3]Cl_2 \cdot EtOH$,[15] 35.40 J K$^{-1}$ mol$^{-1}$ for $[Fe(NCS)_2(phen)_2]$,[5] and 46.1 J K$^{-1}$ mol$^{-1}$ for $[Fe(2\text{-pic})_3]Cl_2 \cdot MeOH$.[11]

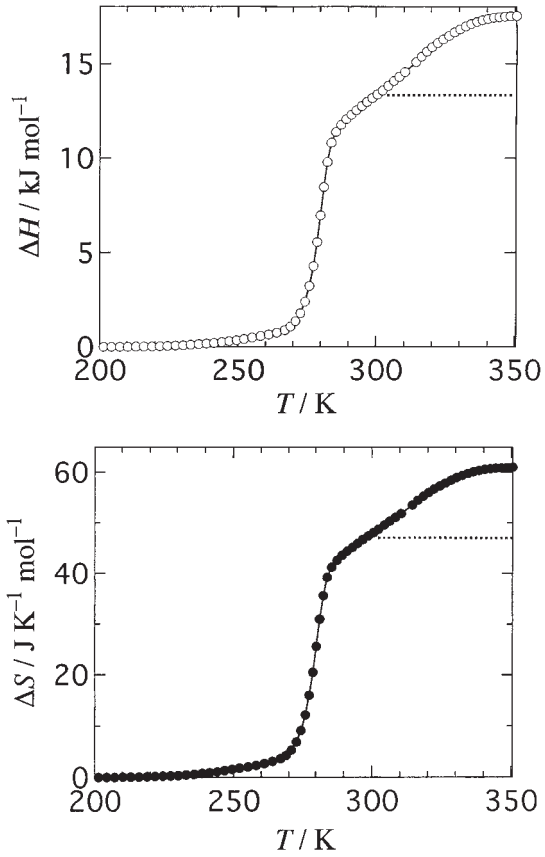


Fig. 11. Plot of transition enthalpy and entropy vs temperature between the stable LS phase and the HS phase.

On the other hand, the enthalpy and entropy gains due to the spin crossover transition from the metastable LS phase (1) to the undercooled HS phase could not be determined in the same manner because of the unexpected stabilization. However, to know the entropy gain from the metastable LS phase (1) to the undercooled HS phase could be of help in discussing the entropy change due to the spin crossover phase transition. In the present case, we assumed that the vertical jumps in the enthalpy and the entropy around at $T_{trs2}$ could be regarded as $\Delta H_{trs}$ and $\Delta S_{trs}$, respectively. Since there were no data for the metastable LS phase (1) around at $T_{trs2}$, the jumps were calculated by using the data at which both the data of the metastable LS phase (1) and the undercooled HS phase were available. Although the temperatures were a little lower than $T_{trs2}$, this method could give a more reliable result than that using the data obtained by extrapolation to $T_{trs2}$. The values thus determined are $\Delta H_{trs} = 8.58$ kJ mol$^{-1}$ and $\Delta S_{trs} = 41.6$ J K$^{-1}$ mol$^{-1}$ at 206.4 K. Interestingly, the entropy change is rather close to the value (47.0 J K$^{-1}$ mol$^{-1}$) gained at the transition from the stable LS to the HS phases excluding the hump.

Finally the phase relationship found for the present complex (see Fig. 12) is discussed. As it is difficult to draw schematically the contribution from the hump centered at 320 K, we neglected it in the Gibbs energy diagram. The phase transition at 280 K was always undercooled to about 200 K (path: A–B–C–D) and the undercooled HS state was transformed to a metastable LS phase (1) around at 200 K (path: D–E). Probably the transi-

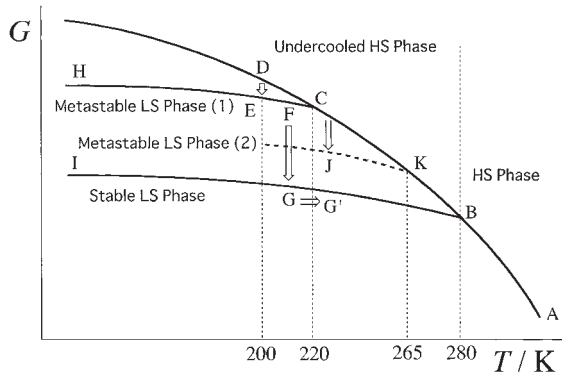


Fig. 12. Schematic drawing of the Gibbs energy relationship between various LS and HS phases realized in $[Fe(2\text{-pic})_3]Cl_2 \cdot H_2O$.

tion causing the hump at 320 K has some relation with this unusually large undercooling. Therefore, the actual curve B–A should not be drawn by a simple curve. When the heating rate is high (the order of a few K $min^{-1}$), this phase was translated to the undercooled HS phase at 211 K (path: E–F–C–B–A). However, when the specimen was treated slowly around this temperature region, it was stabilized to the stable LS phase around at 200 K (path: F–G(G′)). The relaxation time for this stabilization is rather long (the order of ~10 days). Since the time required for data acquisition is extremely long for both Mössbauer spectroscopy and adiabatic calorimetry, the sample was always stabilized, during our experiment, to the stable LS-phase around 200 K. Probably the stabilization occurred during the previous measurement of $^{57}$Fe Mössbauer spectra,[9] but it might be difficult to distinguish the two LS states by Mössbauer spectroscopy. This new finding of the existence of the metastable LS-phase (1) by the present calorimetric study clarified the cause of the apparent thermal hysteresis spanning between 204 K and 295 K found by the Mössbauer experiment, corresponding to the paths A–B–C–D–E–F–G–I and I–G–B–A. Moreover, another intermediate metastable (low-spin?) phase (2) was also found in the course of the measurements by the continuous heating mode with the intermediate heating rates (the order of K $h^{-1}$). When the sample was heated with such rates, some parts of the sample undergo the stabilization to the LS phase (2) (path: C–J) and such a specimen exhibits the phase transition at 265 K (path: E–F–(C)–J–K–B–A). However, the sample was not further stabilized to the stable LS phase, as evidenced by the fact that no thermal anomaly due to the phase transition was observed at ~280 K. Probably, the stabilization from the metastable LS phase (2) to the stable LS has a long relaxation time, so that the sample cannot reach the stable LS phase within a few days.

The standard thermodynamic quantities of $[Fe(2\text{-pic})_3]Cl_2 \cdot H_2O$ have been determined and are tabulated in Tables 4 and 5.

## Concluding Remarks

The new finding of the metastable LS phase by the present calorimetric study disclosed the cause for the unusually large thermal hysteresis of the spin crossover phase transition in

Table 4. Standard Thermodynamic Functions for the Stable Phases of $[Fe(2\text{-pic})_3]Cl_2 \cdot H_2O$ at Rounded Temperatures

| $T$ / K | $C^\circ_{p,m}$ / J·K$^{-1}$·mol$^{-1}$ | $S^\circ_m(T)$ / J·K$^{-1}$·mol$^{-1}$ | $\{H^\circ_m(T) - H^\circ_m(0)\}/T$ / J·K$^{-1}$·mol$^{-1}$ | $-\{G^\circ_m(T) - H^\circ_m(0)\}/T$ / J·K$^{-1}$·mol$^{-1}$ |
|---|---|---|---|---|
| 5 | (0.86) | (0.29) | (0.22) | (0.07) |
| 10 | (6.51) | (2.25) | (1.68) | (0.57) |
| 15 | 17.72 | 6.87 | 5.07 | 1.80 |
| 20 | 30.08 | 13.63 | 9.74 | 3.89 |
| 30 | 57.39 | 30.91 | 21.02 | 9.89 |
| 40 | 84.11 | 51.13 | 33.50 | 17.63 |
| 50 | 109.04 | 72.65 | 46.17 | 26.47 |
| 60 | 131.66 | 94.55 | 58.57 | 35.98 |
| 70 | 152.68 | 116.46 | 70.55 | 45.91 |
| 80 | 172.92 | 138.20 | 82.10 | 56.10 |
| 90 | 190.96 | 159.63 | 93.22 | 66.41 |
| 100 | 207.50 | 180.61 | 103.83 | 76.78 |
| 120 | 238.55 | 221.18 | 123.68 | 97.50 |
| 140 | 270.56 | 260.36 | 142.39 | 117.97 |
| 160 | 300.96 | 298.50 | 160.33 | 138.17 |
| 180 | 331.16 | 335.71 | 177.66 | 158.05 |
| 200 | 362.02 | 372.20 | 194.55 | 177.65 |
| 220 | 393.97 | 408.16 | 211.19 | 196.97 |
| 240 | 432.56 | 444.07 | 228.01 | 216.07 |
| 260 | 477.00 | 480.42 | 245.42 | 235.00 |
| 280 | 1661.9 | 536.83 | 282.72 | 254.11 |
| | | Phase transition(LS → HS) at 280.79 K | | |
| 300 | 657.92 | 596.38 | 321.06 | 275.32 |
| 320 | 697.29 | 640.90 | 344.12 | 296.77 |
| 340 | 642.30 | 681.72 | 363.48 | 318.25 |
| 298.15 | 654.36 | 592.32 | 318.98 | 273.34 |

The values in the parentheses were estimated by extrapolation.

Table 5. Standard Thermodynamic Functions for the Metastable Phases of $[Fe(2\text{-pic})_3]Cl_2 \cdot H_2O$ at Rounded Temperatures

| $T$ | $C^\circ_{p,m}$ | $S^\circ_m(T)$ | $\{H^\circ_m(T) - H^\circ_{m,st}(0)\}/T$ | $-\{G^\circ_m(T) - H^\circ_{m,st}(0)\}/T$ |
|---|---|---|---|---|
| K | $J \cdot K^{-1} \cdot mol^{-1}$ | $J \cdot K^{-1} \cdot mol^{-1}$ | $J \cdot K^{-1} \cdot mol^{-1}$ | $J \cdot K^{-1} \cdot mol^{-1}$ |
| 5 | (1.74) | (0.91) | (1207.4) | (−1206.5) |
| 10 | (7.21) | (3.48) | (605.73) | (−602.25) |
| 15 | 18.07 | 8.35 | 408.00 | −399.65 |
| 20 | 30.41 | 15.19 | 312.01 | −296.82 |
| 30 | 58.00 | 32.77 | 222.79 | −190.02 |
| 40 | 84.93 | 53.20 | 185.00 | −131.81 |
| 50 | 109.34 | 74.82 | 167.47 | −92.65 |
| 60 | 132.20 | 96.79 | 159.71 | −62.92 |
| 70 | 154.47 | 118.82 | 157.34 | −38.51 |
| 80 | 174.06 | 140.79 | 158.26 | −17.47 |
| 90 | 191.33 | 162.32 | 161.01 | 1.31 |
| 100 | 208.47 | 183.39 | 164.92 | 18.47 |
| 120 | 239.29 | 224.08 | 174.71 | 49.37 |
| 140 | 272.71 | 263.47 | 186.32 | 77.15 |
| 160 | 305.51 | 302.07 | 199.21 | 102.86 |
| 180 | 339.69 | 339.95 | 212.85 | 127.11 |
| 200 | 383.93 | 377.88 | 227.60 | 150.28 |
| | | Phase transition (msLS → ucHS) at 220 K | | |
| 220 | 429.67 | 459.59 | 283.51 | 176.08 |
| 240 | 454.75 | 497.98 | 296.67 | 201.31 |
| 260 | 483.63 | 535.51 | 309.93 | 225.58 |
| 280 | 514.18 | 572.46 | 323.42 | 249.04 |
| 300 | 550.76 | 609.24 | 337.41 | 271.83 |
| 320 | 581.96 | 645.79 | 351.73 | 294.06 |
| 340 | 611.65 | 682.32 | 366.49 | 315.83 |
| 298.15 | 547.66 | 605.84 | 336.09 | 269.75 |

The values in the parentheses were estimated by extrapolation. $H^\circ_{m,st}(0)$ means the standard enthalpy of the stable LS phase at 0 K.

$[Fe(2\text{-pic})_3]Cl_2 \cdot H_2O$ reported by the $^{57}$Fe Mössbauer experiment.[9] This large thermal hysteresis spanning between 204 K and 295 K turned out to be not genuine but only apparent. However, this apparent thermal hysteresis provided us with a novel phase cycle consisting of the phase transition from the HS phase to the metastable LS phase at 200 K, the stabilization from the metastable LS phase to the stable LS phase accompanied by a large heat evolution around 200 K, and the final phase transition from the stable LS phase to the HS phase at 280 K. The main reason for the large thermal hysteresis originates in the fact that the HS phase is always undercooled down to ~200 K and transformed to the metastable LS phase. Furthermore, if the heating rate is high, i.e., the order of $K\,min^{-1}$, the metastable LS phase transformed to the undercooled HS phase at around 210 K. It should be noted here that the mechanism of this phenomenon would not be elucidated if the adiabatic calorimetry characterized by extremely long time scale of experiment had not been adopted.

Even though this thermal cycle is not a genuine thermal hysteresis, this phenomenon is very remarkable because the phenomenon does not involve any chemical changes of the compound itself. Namely, the cycle can be repeated by only temperature change just like 'hysteresis'. Contrary to this, there exists a different type of example in which the spin state transformation occurs by a chemical change, such as desolvation from a complex. For example, when a solvated LS complex loses its solvate molecule(s) at high temperature, it may be changed, not always, to a HS complex and thereby may exhibit a spin crossover transition to a LS state at low temperatures. Such a phenomenon has been reported for a iron(II) LS complex $[Fe(hyetrz)_3](3\text{-nitrophenylsulfonate})_2 \cdot 3H_2O$ by Kahn and his collaborators,[16,17] where hyetrz is 4-(2′-hydroxy-ethyl)-1,2,4-triazole. This LS complex experiences a dehydration reaction at 370 K and the dehydrated complex exhibits a HS state. This dehydrated HS form remains stable down to ca. 100 K, where it transforms into a LS form. The authors[16,17] have claimed that this is a non-classical Fe(II) spin crossover behavior leading to an unprecedented extremely large apparent thermal hysteresis of 270 K. However, since the dehydration is an irreversible process, this phenomenon cannot be reproduced by any further thermal treatment. Therefore, it should be remarked here that the spin crossover behavior found for $[Fe(hyetrz)_3](3\text{-nitrophenylsulfonate})_2 \cdot 3H_2O$ does not belong to any thermal hysteresis.

By virtue of precise adiabatic calorimetry, we could provide accurate thermodynamic quantities and we could reveal many new aspects inherent in various types of spin crossover behaviors, initially found by the $^{57}$Fe Mössbauer experiment,[9] in a series of solvated complexes $[Fe(2\text{-pic})_3]Cl_2 \cdot C_2H_5OH$,[15] $[Fe(2\text{-pic})_3]Cl_2 \cdot CH_3OH$,[11] and $[Fe(2\text{-pic})_3]Cl_2 \cdot H_2O$. The remaining problem to be solved is to elucidate the mechanism of the broad heat capacity hump appearing around at 320 K, which will contain a clue to clarify the large undercooling of the HS state beyond the LS-to-HS phase transition at 280.79 K, especially from a structural viewpoint.

This work was partially supported by a Grant-in-Aid for Scientific Research on the Priority Areas of "metal-assembled complexes" (Area No. 401/12023229) from the Ministry of Education, Culture, Sports, Science and Technology.

## References


# Contribution No. 83 from the Research Center for Molecular Thermodynamics. A part of this study has previously been reported in a review article.[1]

1 M. Sorai, *Bull. Chem. Soc. Jpn.*, **74**, 2223 (2001).

2 E. König, *Prog. Inorg. Chem.*, **35**, 527 (1987); *Struct. Bonding*, **76**, 51 (1991).

3 P. Gütlich, A. Hauser, and H. Spiering, *Angew. Chem., Int. Ed. Engl.*, **33**, 2024 (1994).

4 O. Kahn, J. Kröber, and C. Jay, *Adv. Mater.*, **4**, 718 (1992).

5 M. Sorai and S. Seki, *J. Phys. Chem. Solids*, **35**, 555 (1974).

6 S. Decurtins, P. Gütlich, C. P. Köhler, H. Spiering, and A. Hauser, *Chem. Phys. Lett.*, **105**, 1 (1984); S. Decurtins, P. Gütlich, C. P. Köhler, H. Spiering, and A. Hauser, *J. Chem. Soc., Chem. Commun.*, **1985**, 430; S. Decurtins, P. Gütlich, K. M. Hasselbach, H. Spiering, and A. Hauser, *Inorg. Chem.*, **24**, 2174 (1985).

7 J. Kröber, E. Codjovi, O. Kahn, F. Grolière, and C. Jay, *J. Am. Chem. Soc.*, **115**, 9810 (1993).

8 Z. J. Zhong, J.-Q. Tao, Z. Yu, C.-Y. Dun, Y.-J. Liu, and X. Z. You, *J. Chem. Soc., Dalton Trans.*, **1998**, 327.

9 M. Sorai, J. Ensling, K. M. Hasselbach, and P. Gütlich, *Chem. Phys.*, **20**, 197 (1977).

10 B. A. Katz and C. E. Strouse, *Inorg. Chem.*, **19**, 658 (1980).

11 T. Nakamoto, Z.-C. Tan, and M. Sorai, *Inorg. Chem.*, **41**, 3805 (2001).

12 M. Sorai, A. Nishimori, and Y. Nagano, unpublished.

13 T. Preston-Thomas, *Metrologia*, **27**, 107 (1990).

14 M. Sorai and S. Seki, *J. Phys. Soc. Jpn.*, **32**, 382 (1972).

15 K. Kaji and M. Sorai, *Thermochim. Acta*, **88**, 185 (1985).

16 Y. Garcia, P. J. van Koningsbruggen, E. Codjovi, R. Lapouyade, O. Kahn, and L. Rabardel, *J. Mater. Chem.*, **7**, 857 (1997).

17 P. J. van Koningsbruggen, Y. Garcia, E. Codjovi, R. Lapouyade, O. Kahn, L. Fournès, and L. Rabardel, *J. Mater. Chem.*, **7**, 2069 (1997).